OPTOELECTRONICS AND ADVANCED MATERIALS – RAPID COMMUNICATIONS Vol. 19, Iss. 3-4, March-April 2025, p. 202 - 210

Performance improvement of simplified $CsPbBr_3$ perovskite solar cell with doping $BaBr_2$

FEI ZHAO[1,*], YIXIN GUO[2,*], QIMING YANG[3], PEIZHI YANG[3], JUNHAO CHU[4]
[1]*School of Photoelectric Engineering, Changzhou Institute of Technology, Changzhou, Jiangsu, 213032, China*
[2]*Department of Physics, Shanghai Normal University, Shanghai 200233, China*
[3]*Key Laboratory of Advanced Technique & Preparation for Renewable Energy Materials, Ministry of Education, Yunnan Normal University, Kunming 650500, China*
[4]*Shanghai Institute of Technical Physics, Chinese Academy of Sciences, Shanghai 200083, China*

All-inorganic $CsPbBr_3$ perovskite solar cells have attracted increasing attention due to their long-term stability. Here, all-inorganic $CsPbBr_3$ perovskites are doped with $BaBr_2$ to improve the efficiency of perovskite solar cells. The $CsPbBr_3$ perovskite film displays better crystallinity, higher valence band maximum (VBM) position and lower carrier recombination probability after introducing $BaBr_2$. Hence, the electron-hole transport layer-free device with the presence of $BaBr_2$ achieves the improvement of the efficiency and stability. In particular, the efficiency of the device enhances from 1.88% to 2.86% by optimizing the doping concentration of $BaBr_2$. In addition, the $BaBr_2$-doped device without encapsulation exhibits excellent performance in air with relative humidity of ~80%.

(Received August 16, 2024; accepted April 3, 2025)

Keywords: Doping $BaBr_2$, Simplified structure, $CsPbBr_3$ perovskite solar cells, Photovoltaic performance

1. Introduction

Hybrid perovskite materials have caused widespread attention due to their high absorption coefficient and adjustable band gap [1-5]. Moreover, their simple preparation method, namely solution processes, and vapor deposition technologys, enables the application of hybrid perovskite materials in the field of solar cell devices [6-8]. Even more surprisingly, the hybrid perovskite solar cells obtain a high efficiency of 26.1% [9]. Nevertheless, the main problems in their commercial application are the inferior stability of the organic cations in the halide perovskites against humidity and high temperature [10-14]. In contrast, all-inorganic perovskite materials based on excellent stability to moisture have been successfully applied in photovoltaic cells in the past few years.

The all-inorganic perovskite solar cells include $CsSnI_3$ [15], $CsPbI_3$ [16], $CsPbI_2Br$ [17], $CsPbIBr_2$ [18] and $CsPbBr_3$ [4] devices. Among these all-inorganic devices, the $CsPbBr_3$ cell possesses the best stability [19]. Liang et al. adopted the compact TiO_2 electronic transport layer (ETL) in all-inorganic $CsPbBr_3$ cells and realized an efficiency of 3.6% [20]. Afterwards, Teng et al. used the TiO_2 film as ETL for the $CsPbBr_3$ cells and delivered an efficiency of 5.86% [21]. Our group prepared all-inorganic $CsPbBr_3$ cell with Nb_2O_5 ETL, and the efficiency of 5.12% was gained [22]. Liu et al. introduced Cu-Phthalocyanine as hole transport layer (HTL) in carbon counter electrode-based $CsPbBr_3$ cell and gained a great efficiency of 6.21% [23]. Wang et al. prepared carbon-based $CsPbBr_3$ device based on P3HT HTL and it had a high conversion efficiency (6.49%) [24]. In the above article, the ETL and HTL are applied in all-inorganic $CsPbBr_3$ cells. The TiO_2 and Nb_2O_5 ETLs require high-temperature sintering at 500 °C to improve crystallinity and carrier transfer ability. However, this leads to high energy consumption and cumbersome procedures. Thus, this high-temperature processing for ETLs is inapplicable for manufacturing plastic devices [25]. Despite significant efforts have been made to lower heating temperature below 100 °C or to replace TiO_2 and Nb_2O_5 with other ETLs, the tedious procedure in the device manufacturing process is still a challenge to guarantee the good contact with the substrate [26]. In addition, the above-mentioned HTLs require high prices, which limits the commercial application of the devices. Duan et al. fabricated the simplified $CsPbBr_3$ perovskite cell without ETL and HTL [27]. They obtained a conversion efficiency of 2.35%. However, this efficiency value is relatively low and needs further improvement.

In this work, we modify the structure and morphology of $CsPbBr_3$ films by doping $BaBr_2$. We found that the introduction of $BaBr_2$ can significantly enhance the crystallinity and VBM energy level position of $CsPbBr_3$ absorbers. Meanwhile, the number of grain boundaries and the recombination probability of charge carriers are reduced after doping $BaBr_2$. FTO/$CsPbBr_3$/C cells were assembled to simplify the manufacturing process and reduce the cost. Compared with the pristine $CsPbBr_3$ cell, the $BaBr_2$-doped $CsPbBr_3$ cell can achieve a higher efficiency of 2.86%. Furthermore, the $BaBr_2$-doped devices under unpackaged conditions present prominent durability in atmosphere with a relative humidity of about 80%.

2. Experimental

2.1. Deposition of solar cells

All manufacturing processes of $CsPbBr_3$ cells are carried out at room temperature and ambient air. Fluorine-doped tin oxide (FTO) glass was ultrasonic rinsed with deionized water, ethanol, acetone, and isopropanol. The $CsPbBr_3$ film was prepared via multi-step spin-coating method. In details, 367 mg/ml $PbBr_2$ (99.999%) in N,N-dimethylformamide (DMF, 99.8%) solution was spin-coated on FTO at 2000 rpm for 30s and heated at 90 °C for 30 min. Afterwards, 15 mg/ml CsBr (99.999%) methanol solution (99.9%) was spin-coated on $PbBr_2$ at 2000 rpm for 30s, and dried at 250 °C for 5 min. The $CsPbBr_3$ film was synthesized via repeatedly coating CsBr for four times. $BaBr_2$ (99.99%) doped perovskite cell was prepared through adding the certain $BaBr_2$ (12 mg and 18 mg) to $PbBr_2$ solution. The rest processes followed the standard procedure. The device was manufactured via coating carbon paste on the $CsPbBr_3$ film and heating on a hot plate at 120 °C for 15 min.

2.2. Characterizations

The crystallinity of $CsPbBr_3$ film was gained via X-ray diffraction (XRD). The surface morphology of $CsPbBr_3$ film was obtained via scanning electron microscopy (SEM). The chemical valence state of $CsPbBr_3$ film was measured through X-ray photoelectron spectroscopy (XPS). The absorption rate and optical band gap of $CsPbBr_3$ films were tested through UV-VIS-NIR spectrophotometer. The energy level position of $CsPbBr_3$ film was obtained by ultraviolet photoelectron spectra (UPS). The carrier transport and recombination properties of $CsPbBr_3$ films were tested by steady-state photoluminescence (PL) and time resolved photoluminescence (TRPL) spectra. The current density-voltage (J-V) curve was tested under AM 1.5 (100 mW/cm^2). The incident photo-to-current conversion efficiency (IPCE) was gained. The $CsPbBr_3$ solar cell was masked with a 0.09 cm^2 active area.

3. Results and discussions

3.1. Analysis of $CsPbBr_3$ perovskite film

Fig. 1a shows the XRD patterns of all-inorganic perovskites. The $CsPbBr_3$ films without and with doping $BaBr_2$ present two characteristic diffraction peaks at $2\theta=21.67^\circ$ and 30.70°, corresponding to (110) and (200) crystal planes of perovskite films [28]. The characteristic peak at $2\theta=26.51^\circ$ corresponds to FTO [29]. The absence of peaks in the impurity phase indicates that the perovskite film has high purity by employing the method reported in this work. Compared with $CsPbBr_3$ films without doping $BaBr_2$, $BaBr_2$-doped $CsPbBr_3$ films have stronger main peak of (110) crystal plane. The stronger peak shows that $CsPbBr_3$ film possesses better crystallinity [30]. In comparison to $CsPbBr_3$ without doping $BaBr_2$, the diffraction peaks shift to lower angles for $BaBr_2$-doped $CsPbBr_3$ (Fig. 1b). The reasonable mechanism behind this phenomenon can be explained via the deviation of ionic radius between Pb^{2+} (1.190Å) and Ba^{2+} (1.350 Å), resulting in the lattice expansion of the $CsPbBr_3$ perovskite film [31,32]. Fig. 1c shows XPS spectra for Pb 4f peaks. As expected, the high-resolution XPS spectra of Pb 4f shift to lower binding energy via doping larger Ba ions [33]. This indicates that Ba ions are successfully doped into the lattice of $CsPbBr_3$ perovskite films. From Fig. 1d, it can be seen that the $CsPbBr_3$ films with doping $BaBr_2$ present characteristic peak of Ba 3d. This also suggests that Ba ions are incorporated into $CsPbBr_3$ perovskite films, which is consistent with the above results.

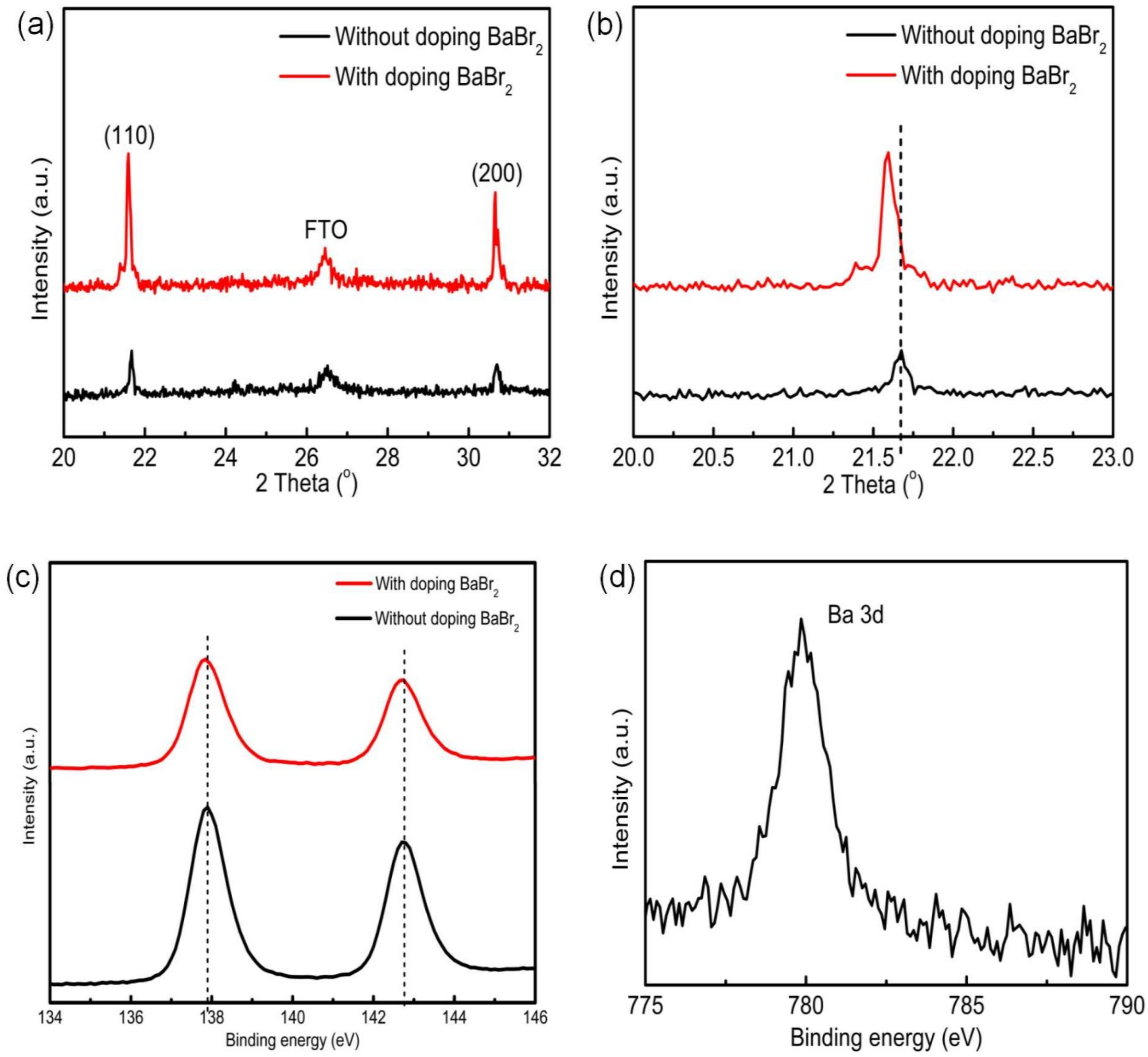

Fig. 1. (a) XRD patterns and (b) local magnified XRD images of $CsPbBr_3$ perovskite films without and with doping $BaBr_2$; (c) XPS spectra for Pb 4f peaks; (d) Ba 3d spectrum of $CsPbBr_3$ film with doping $BaBr_2$ (colour online)

The surface morphology of $CsPbBr_3$ films without and with doping $BaBr_2$ can be evaluated by SEM measurement, as shown in Fig. 2a and b. The top-view SEM image of the pristine $CsPbBr_3$ film exhibits some small grains and some grain boundaries, largely due to its lower crystallinity. By contrast, the $BaBr_2$-doped $CsPbBr_3$ film presents some larger grains and some less grain boundaries. The reduction of grain boundaries can dilute the density of defects, thereby reducing the charge recombination losses [34]. Fig. 2c presents the absorption rate for the pristine $CsPbBr_3$ and $BaBr_2$-doped $CsPbBr_3$ films. The $BaBr_2$-doped $CsPbBr_3$ film exhibits enhanced absorption in comparsion to the pristine $CsPbBr_3$ film, which is beneficial for absorbing more sunlight to improve the performance of $CsPbBr_3$ solar cell [35]. Fig. 2d indicates the band gaps of $CsPbBr_3$ films without and with doping $BaBr_2$. As seen in Fig. 2d, the $BaBr_2$-doped $CsPbBr_3$ displays the same band gap of 2.34 eV with pristine $CsPbBr_3$ film, showing small amount Ba substitution possesses a negligible influence on the band gap of $CsPbBr_3$ film.

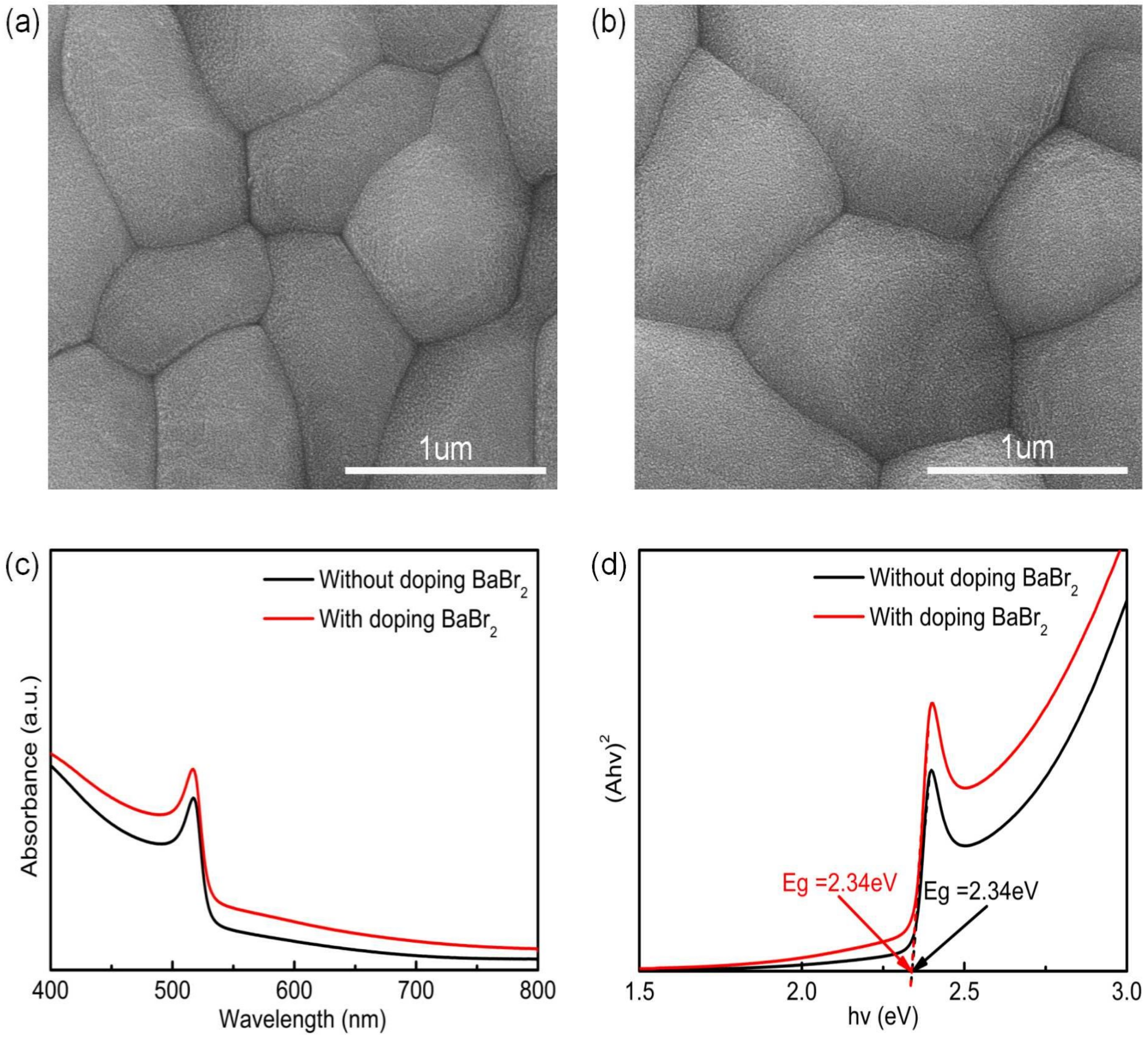

Fig. 2. Top-view SEM images of $CsPbBr_3$ (a) without doping $BaBr_2$ and (b) with doping $BaBr_2$. (c) absorption spectra and (d) band gaps of $CsPbBr_3$ films without and with doping $BaBr_2$ (colour online)

3.2. Analysis of $CsPbBr_3$ solar cell

The cross-sectional SEM image for $CsPbBr_3$ solar cell is shown in Fig. 3a. From Fig. 3a, it can be seen that the $CsPbBr_3$ device is composed of FTO, perovskite absorber and carbon electrode. There are no holes and the contact is tight at the interfaces of FTO/$CsPbBr_3$ and $CsPbBr_3$/carbon electrode, indicating that the quality of the $CsPbBr_3$ device is great [36]. In order to investigate the effect of doping $BaBr_2$ on the energy band structure of $CsPbBr_3$ film, UPS measurement is evaluated, as seen in Fig. 3(b-e). Fig. 3(b-e) indicate the secondary electron cutoff edge (E_{cutoff}) and Fermi edge of $CsPbBr_3$ films without and with doping $BaBr_2$, separately. The Fermi level values of $CsPbBr_3$ films without and with doping $BaBr_2$ can be gained via subtracting the intercept of the Fermi edge from the He excitation energy [37]. The valence band maximum (VBM) and conduction band minimum (CBM) can be gained via employing E_{cutoff}, Fermi level values and band gaps of $CsPbBr_3$ films without and with doping $BaBr_2$. Fig. 3f manifests the energy level diagram for solar cells based on the pristine and $BaBr_2$-doped $CsPbBr_3$ absorbers. As shown in Fig. 3f, the VBM of $BaBr_2$-doped $CsPbBr_3$ film is closer to the Fermi level of carbon electrode in comparsion to pristine $CsPbBr_3$ film. The VBM is close to the Fermi level of the carbon electrode, which is beneficial for increasing the open circuit voltage of the $CsPbBr_3$ device [38].

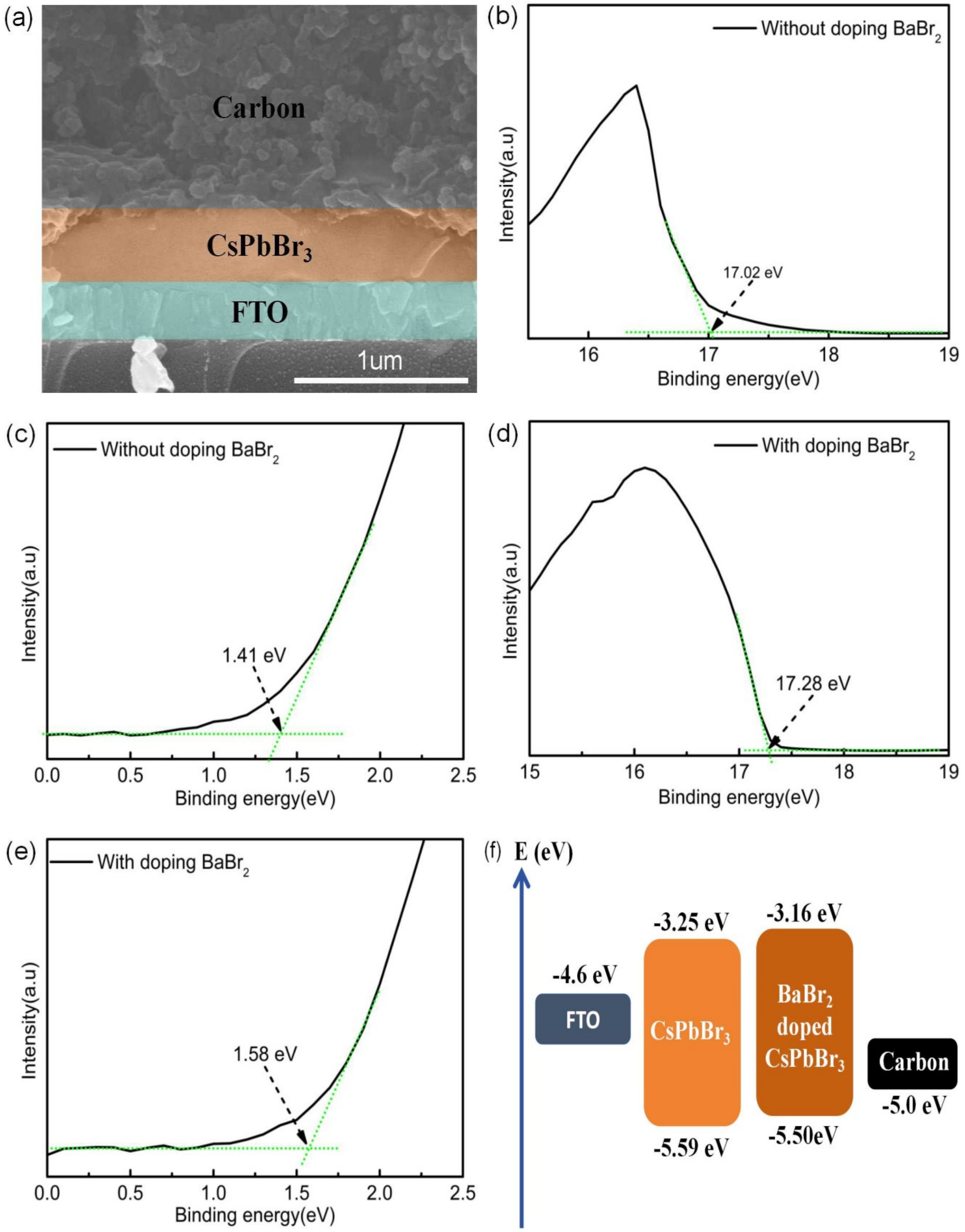

Fig. 3. (a) Cross-sectional SEM image of $CsPbBr_3$ solar cell. (b) Fermi edge of $CsPbBr_3$ film without doping $BaBr_2$. (c) Secondary electron cutoff edge of $CsPbBr_3$ film without doping $BaBr_2$. (d) Fermi edge of $CsPbBr_3$ film with doping $BaBr_2$. (e) Secondary electron cutoff edge of $CsPbBr_3$ film with doping $BaBr_2$. (f) Energy level diagram for $CsPbBr_3$ devices without and with doping $BaBr_2$ (colour online)

The champion J-V curves and photovoltaic parameters of $CsPbBr_3$ solar cells with different $BaBr_2$ contents are presented in Fig. 4a and Table 1. The $CsPbBr_3$ cell without doping $BaBr_2$ displays a comparatively low efficiency of 1.88% including an open circuit voltage (V_{oc}) of 1.089 V, a short-circuit current density (J_{sc}) of 3.90 mA/cm^2 and a fill factor (FF) of 44.23%. When $BaBr_2$ content is 12 mg, the V_{oc}, J_{sc} and FF of the $CsPbBr_3$ device obviously increases to 1.176V, 4.54 mA/cm^2 and 53.66%, separately. As the content of $BaBr_2$ increases to 18 mg, the photovoltaic parameters of the device decreases comprehensively. Therefore, the photovoltaic performance of the device is optimal when the $BaBr_2$ content is 12 mg. Compared with the $CsPbBr_3$ devices with 0 mg and 18 mg $BaBr_2$, the $CsPbBr_3$ device with 12 mg $BaBr_2$ has a better photovoltaic performance. The improvement of photovoltaic performance for $CsPbBr_3$ device with 12 mg $BaBr_2$ mainly refers to the enhancement of V_{oc}, J_{sc}, and FF. The improvement in V_{oc} is attributed to higher VBM. The increase of J_{sc} is due to the higher crystallinity and fewer grain boundaries of perovskite films. To assure the reproducibility of device, average efficiencies for 30 devices without and with doping $BaBr_2$ are tested and are seen in Fig. 4b. The $CsPbBr_3$ cell with doping $BaBr_2$ indicates an average efficiency of 2.48%, which is higher than that of $CsPbBr_3$ cell without doping $BaBr_2$ (1.36%). The above results indicate that our device possess excellent repeatability [39].

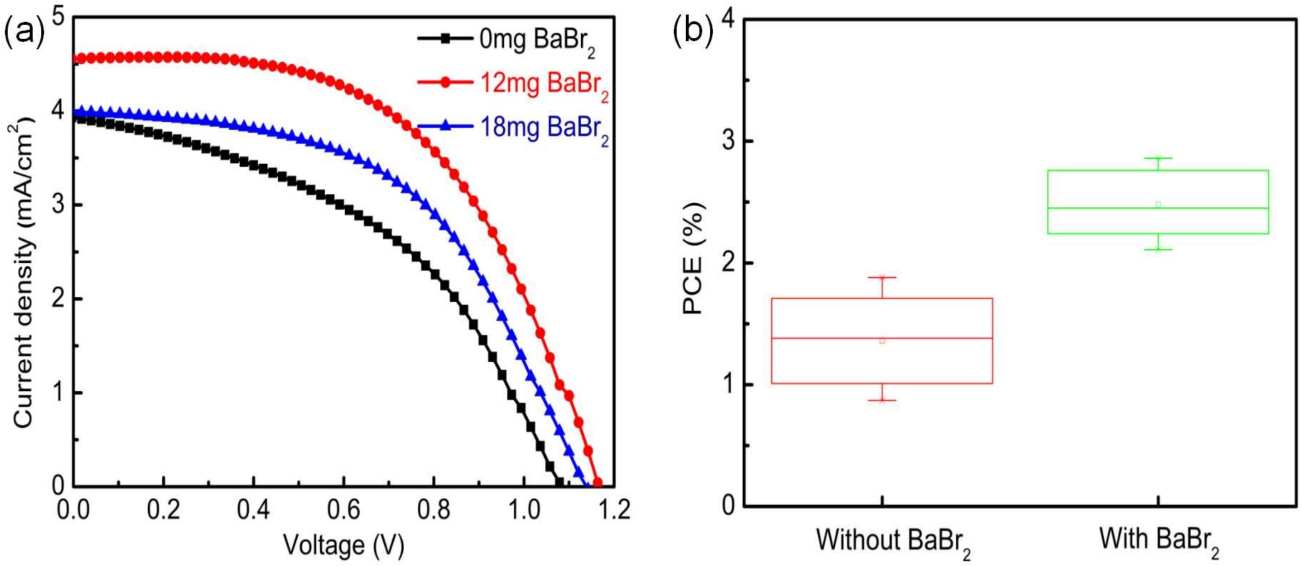

Fig. 4. (a) J-V curves for $CsPbBr_3$ devices without and with doping $BaBr_2$. (b) Average PCEs for 30 devices without and with doping $BaBr_2$ (colour online)

Table 1. Photovoltaic parameters for $CsPbBr_3$ devices without and with doping $BaBr_2$

Sample	V_{oc}(V)	J_{sc}(mA/cm^2)	FF(%)	PCE(%)
0 mg $BaBr_2$	1.089	3.90	44.23	1.88
12 mg $BaBr_2$	1.176	4.54	53.66	2.86
18 mg $BaBr_2$	1.138	3.98	51.85	2.35

To study the charge dynamics of the pristine $CsPbBr_3$ film and the $BaBr_2$-doped $CsPbBr_3$ film, we carried TRPL measurements. The TRPL decay curves of the pristine $CsPbBr_3$ and the $BaBr_2$-doped $CsPbBr_3$ films seen in Fig. 5a are used to obtain carrier lifetime through Equation (1):

$$f(t)=A_1\exp(-t/\tau_1)+A_2\exp(-t/\tau_2)+B, \qquad (1)$$

Typically, A_1 and A_2 represent the relative amplitudes, B represents offset value, τ_1 reflects the information for the interface recombination process, and τ_2 represents the information for the bulk recombination process [40]. The average carrier lifetime τ_{ave} is gained by Equation (2):

$$\tau_{ave}=\sum A_i\tau_i/\sum A_i, \qquad (2)$$

The pristine $CsPbBr_3$ sample displays a τ_{ave} of 18.63ns. However, the τ_{ave} is extended to 40.99ns for the $BaBr_2$-doped $CsPbBr_3$ sample. This suggests lower trap states in $CsPbBr_3$ film with doping $BaBr_2$, thus it has a superior charge transfer performance [41].

Fig. 5b plots the V_{oc} outputs from various cells as a function of light intensity. The relationship between V_{oc} and light intensity can be studied by the Equation (3):

$$V_{oc}=nkT\ln(I)/q+\text{constant}, \qquad (3)$$

where n stands for the ideal factor, k stands for the Boltzmann constant, T stands for the absolute temperature, and q stands for the basic charge. An n value as high as 2.518 is obtained for FTO/pristine $CsPbBr_3$/carbon cell, and it reduces to 2.194 for FTO/ $BaBr_2$-doped $CsPbBr_3$ /carbon cell. Namely, trap-assisted non-radiative recombination is partially eliminated [42]. Therefore, we can conclude that doping $BaBr_2$ can effectively suppress charge recombination, which enhances the V_{oc}, J_{sc} and FF of the $CsPbBr_3$ cell.

Long-term stability is a significant aspect for $CsPbBr_3$-based cells. Fig. 5c manifests time-dependent normalized efficiency for cells stored in air with a high relative humidity of ~80% at 25 °C. It can be seen that $CsPbBr_3$ cell without $BaBr_2$ can maintain 70% of its initial efficiency after storage for 10 days. However, $CsPbBr_3$ cell with doping $BaBr_2$ can keep 78% of its initial efficiency under the same storage conditions. The reason behind the improvement in device stability is that doping $BaBr_2$ can enhance the crystallinity of perovskite films and reduce their number of grain boundaries [43]. Fig. 5d shows the normalized PCE of the device with doping $BaBr_2$ after storing in the air (~80% humidity, 25 °C) for 30 days. From Fig. 5d, it can be seen that after storing for 30 days, the device with doping $BaBr_2$ can maintain 52% of its initial efficiency.

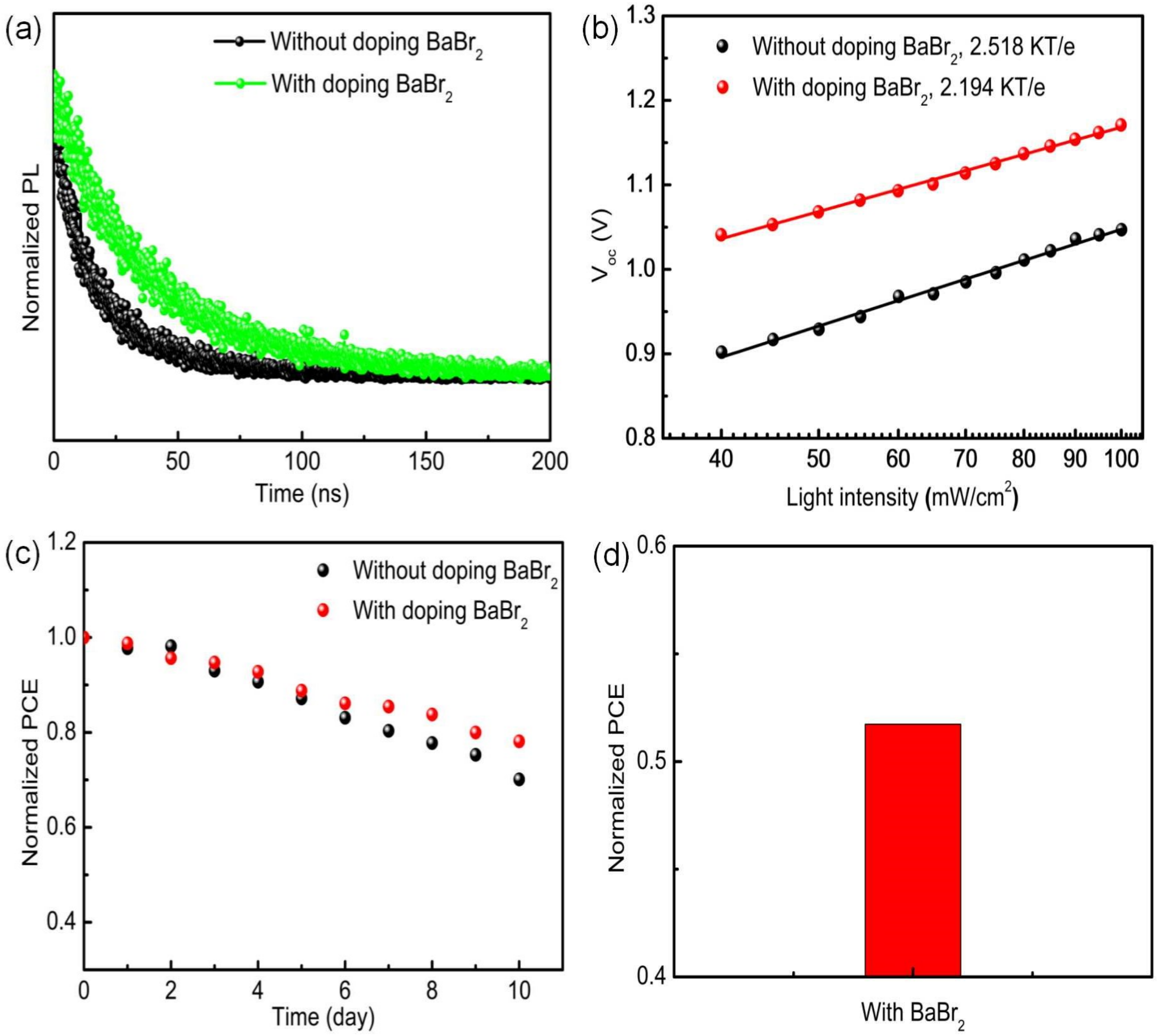

Fig. 5. (a) TRPL spectra of $CsPbBr_3$ films without and with doping $BaBr_2$. (b) V_{oc} dependence on light intensity of $CsPbBr_3$ devices without and with doping $BaBr_2$. (c) Durability of the devices when stored in the atmosphere with a humidity of ~80% at 25 °C. (d) Normalized PCE of the device with doping $BaBr_2$ after storing in the air (~80% humidity, 25 °C) for 30 days (colour online)

4. Conclusions

In this study, the solar cells of FTO/$CsPbBr_3$/Carbon structure are successfully prepared under air environment. The charge extraction between the $CsPbBr_3$ absorbing layer and Carbon is improved by incorporating $BaBr_2$ in the $CsPbBr_3$ absorbing layer. The introduction of $BaBr_2$ can adjust the energy band structure of $CsPbBr_3$ to reduce the high energy barrier between the $CsPbBr_3$ absorption layer and the carbon electrode. Therefore, the hole transport ability from the absorbing layer to the carbon electrode is stronger. The efficiency of $CsPbBr_3$ solar cell is increased from 1.88% to 2.86% after doping $BaBr_2$. The $CsPbBr_3$ cell with a small amount of Ba ions exhibits better environmental stability. The unpackaged devices with doping $BaBr_2$ can maintain more than 78% of the initial efficiency after storing in the air for 10 days.

Acknowledgements

This work was financed by the National Natural Science Foundation of China (Grant No. 12304043), the Key Applied Basic Research Program of Yunnan Province (Grant No. 202201AS070023) and Yunnan Revitalization Talent Support Program, the Spring City Plan: the High-level Talent Promotion and Training Project of Kunming (Grant No. 2022SCP005).

References

[1] J. Liang, J. Liu, Z. Jin, Sol. RRL **1**, 1700086 (2017).
[2] D. Yang, X. Zhou, R. Yang, Z. Yang, W. Yu, X. Wang, C. Li, S. Liu, R. P. H. Chang, Energy Environ. Sci. **9**, 3071 (2016).
[3] B. Saparov, F. Hong, J. Sun, H. Duan, W. Meng, S. Cameron, I. G. Hill, Y. Yan, D. B. Mitzi, Chem. Mater. **27**, 5622 (2015).
[4] N. Ishida, A. Wakamiya, A. Saeki, ACS Photonics **3**, 1678 (2016).
[5] F. De Rossi, G. Renno, B. Taheri, N. Y. Nia, V. Ilieva, A. Fin, A. D. Carlo, M. Bonomo, C. Barolo, F. Brunetti, J. Power Sources **494**, 229735 (2021).
[6] Q. Chen, H. Zhou, Z. Hong, S. Luo, H. S. Duan, H. H. Wang, Y. Liu, G. Li, Y. Yang, J. Am. Chem. Soc. **136**, 622 (2014).
[7] M. Liu, M. B. Johnston, H. J. Snaith, Nature **501**, 395 (2013).
[8] N. J. Jeon, J. H. Noh, Y. C. Kim, W. S. Yang, S. Ryu, S. I. Seok, Nat. Mater. **13**, 897 (2014).
[9] H. Dong, Z. Wang, Q. Zhang, Z. Zhang, Z. Zhu, X. Han, J. Gu, X. Wang, J. Yang, T. Yu, C. Bao, Z. Zou, Appl. Phys. Lett. **124**, 173903 (2024).
[10] H. Yuan, Y. Zhao, J. Duan, B. He, Z. Jiao, Q. Tang, Electrochim. Acta **279**, 84 (2018).
[11] L. Zhou, M. Sui, J. Zhang, K. Cao, H. Wang, H. Yuan, Z. Lin, J. Zhang, P. Li, Y. Hao, J. Chang, Chem. Eng. J. **496**, 154043 (2024).
[12] J. Chen, Z. Wu, S. Chen, W. Zhao, Y. Zhang, W. Ye, R. Yang, L. Gong, Z. Peng, J. Chen, Mat. Sci. Semicon. Proc. **174**, 108186 (2024).
[13] Y. Xu, C. Yan, H. Liang, S. Huang, P. Feng, J. Song, Nanotechnology **35**, 175404 (2024).
[14] X. Jiang, C. Geng, X. Yu, J. Pan, H. Zheng, C. Liang, B. Li, F. Long, L. Han, Y. Cheng, Y. Peng, ACS Appl. Mater. Interfaces **16**, 19039 (2024).
[15] M. H. Kumar, S. Dharani, W. L. Leong, P. P. Boix, R. R. Prabhakar, T. Baikie, C. Shi, H. Ding, R. Ramesh, M. Asta, M. Graetzel, S. G. Mhaisalkar, N. Mathews, Adv. Mater. **26**, 7122 (2014).
[16] A. Swarnkar, A. R. Marshall, E. M. Sanehira, B. D. Chernomordik, D. T. Moore, J. A. Christians, T. Chakrabarti, J. M. Luther, Science **354**, 92 (2016).
[17] R. J. Sutton, G. E. Eperon, L. Miranda, E. S. Parrott, B. A. Kamino, J. B. Patel, M. T. Horantner, M. B. Johnston, A. A. Haghighirad, D. T. Moore, H. J. Snaith, Adv. Energy Mater. **6**, 1502458 (2016).
[18] C. F. Lau, X. F. Deng, Q. S. Ma, J. S. Zheng, S. J. Yun, M. A. Green, S. J. Huang, A. W. Baillie, ACS Energy Lett. **1**, 573 (2016).
[19] G. Liao, J. Duan, Y. Zhao, Q. Tang, Sol. Energy **171**, 279 (2018).
[20] J. Liang, C. Wang, Y. Wang, Z. Xu, Z. Lu, Y. Ma, H. Zhu, Y. Hu, C. Xiao, X. Yi, G. Zhu, H. Lv, L. Ma, T. Chen, Z. Tie, Z. Jin, J. Liu, J. Am. Chem. Soc. **138**, 15829 (2016).
[21] P. Teng, X. Han, J. Li, Y. Xu, L. Kang, Y. Wang, Y. Yang, T. Yu, ACS Appl. Mater. Interfaces **10**, 9541 (2018).
[22] F. Zhao, Y. Guo, X. Wang, J. Tao, J. Jiang, Z. Hu, Junhao Chu, Sol. Energy **191**, 263 (2019).
[23] Z. Liu, B. Sun, X. Liu, J. Han, H. Ye, T. Shi, Z. Tang, G. Liao, Nano-Micro Lett. **10**, 34 (2018).
[24] G. Wang, W. Dong, A. Gurung, K. Chen, F. Wu, Q. He, R. Pathak, Q. Qiao, J. Power Sources **432**, 48 (2019).
[25] S. Shin, W. Yang, J. Noh, J. Suk, N. Jeon, J. Park, J. Kim, W. Seong, S. Seok, Nat. Commun. **6**, 7410 (2015).
[26] J. Wang, J. Ball, E. Barea, A. Abate, J. Alexander-Webber, J. Huang, M. Saliba, I. Mora-Sero, J. Bisquert, H. Snaith, R. Nicholas, Nano Lett. **14**, 724 (2014).
[27] J. Duan, Y. Zhao, B. He, Q. Tang, Small **14**, 1704443 (2018).
[28] X. Liu, X. Tan, Z. Liu, H. Ye, B. Sun, T. Shi, Z. Tang, G. Liao, Nano Energy **56**, 184 (2019).
[29] F. Zhao, Y. Guo, J. Tao, Z. Li, J. Jiang, J. Chu, Appl. Optics **59**, 5481 (2020).
[30] T. Singh, S. Öz, A. Sasinska, R. Frohnhoven, S. Mathur, T. Miyasaka, Adv. Funct. Mater. **28**, 1706287

(2018).

[31] H. Liu, Z. Wu, J. Shao, D. Yao, H. Gao, Y. Liu, W. Yu, H. Zhang, B. Yang, ACS Nano **11**, 2239 (2017).

[32] J. Liang, Z. Liu, L. Qiu, Z. Hawash, L. Meng, Z. Wu, Y. Jiang, L. K. Ono, Y. Qi, Adv. Energy Mater. **8**, 1800504 (2018).

[33] Y. Zhao, Y. Wang, J. Duan, X. Yang, Q. Tang, J. Mater. Chem. A **7**, 6877 (2019).

[34] G. Tong, T. Chen, H. Li, L. Qiu, Z. Liu, Y. Dang, W. Song, L. K. Ono, Y. Jiang, Y. Qi, Nano Energy **65**, 104015 (2019).

[35] Z. Xu, X. Yin, Y. Guo, Y. Pu, M. He, J. Mater. Chem. C **6**, 4746 (2018).

[36] J. Zhu, B. He, X. Yao, H. Chen, Y. Duan, J. Duan, Q. Tang, Small **18**, 2106323 (2022).

[37] Y. Guo, J. Jiang, S. Zuo, F. Shi, J. Tao, Z. Hu, X. Hu, G. Hu, P. Yang, J. Chu, Sol. Energy Mater. Sol. Cell. **178**, 186 (2018).

[38] H. Guo, Y. Pei, J. Zhang, C. Cai, K. Zhou, Y. Zhu, J. Mater. Chem. C **7**, 11234 (2019).

[39] Z. Zhang, W. Zhu, T. Han, T. Wang, W. Chai, J. Zhu, H. Xi, D. Chen, G. Lu, P. Dong, J. Zhang, C. Zhang, Y. Hao, Energy Environ. Mater. **7**, e12524 (2024).

[40] Y. Guo, F. Zhao, J. Tao, J. Jiang, J. Zhang, J. Yang, Z. Hu, J. Chu, ChemSusChem **12**, 983 (2019).

[41] C. F. J. Lau, M. Zhang, X. Deng, J. Zheng, J. Bing, Q. Ma, J. Kim, L. Hu, M. A. Green, S. Huang, ACS Energy Lett. **2**, 2319 (2017).

[42] F. Zhao, Y. Guo, X. Wang, J. Tao, Z. Li, D. Zheng, J. Jiang, Z. Hu, J. Chu, J. Alloy. Compd. **842**, 155984 (2020).

[43] Y. Wang, A. Tong, Y. Wang, K. Liang, W. Zhu, Y. Wu, W. Sun, J. Wu, Mater. Today Chem. **40**, 102228 (2024).

---

[*] Corresponding author: fzhaobs@126.com;
yxguo@shnu.edu.cn